Astron. Astrophys. 322, 659–670 (1997)

ASTRONOMY AND ASTROPHYSICS

Acoustic waves in isothermal winds in the vicinity of the sonic point

Roland Grappin[1], **Etienne Cavillier**[1], **and Marco Velli**[2]

[1] Observatoire de Paris-Meudon, F-92195 Meudon, France and CNRS, ASCI, Orsay, France
[2] Dipartimento di Astronomia, Universita di Firenze, Italy

Recieved 10 May 1996 / Accepted 9 August 1996

Abstract. We study the propagation of acoustic waves incident on the base of a stellar wind and the back-reaction on the mean flow, in the spherically symmetric, isothermal case, both analytically and via direct simulations of the Navier-Stokes equations. We consider successively the quasi-linear inviscid case and the nonlinear dissipative case (shocks). We show that wave reflection is small everywhere even when the WKB approximation breaks down, and conjecture that the same result could hold for radial Alfvén waves in a spherically symmetric wind. We show that, after a transient acceleration, outward propagating waves lead to a lower mean wind velocity than in the unperturbed wind, so that the average velocity may become negative below the sonic point, the difference with the standard result that Lagrangian-mean velocities are higher in presence of waves being explained by the drift between reference frames. We propose that negative average velocities might provide a test for the presence of compressive waves close to the sun. We conjecture that, for MHD fluctuations, the net effect of the wave pressure on the wind velocity depends on the importance of compressive components, and that this might play a role in the observed correlation between the mean solar wind velocity and the level of the compressive component in the wave spectrum.

Key words: hydrodynamics – Sun: solar wind – MHD – waves

1. Introduction

What is the origin of the solar wind turbulent state, and what is the back-reaction of turbulence on the mean flow? The spectrum measured in situ shows at large-scale a stream structure, and then a wave range, which appears to a large extent (at least in the fast streams far from the ecliptic plane) to be made of Alfvén waves, which are possibly the remnants of waves driving the fast winds. Although a direct assessment is impossible, compressive propagating waves are thought to be a minor component in the region of the heliosphere where in situ measurements have been made. Closer to the sun however, acoustic waves might play a more important role. Indeed, the amplitude of acoustic waves propagating upward in the stratified part of the atmosphere grows rapidly (Parker, 1966), and their subsequent dissipation should lead to a well-defined peak in amplitude. The observed peak in turbulent activity in the acceleration region (Scott et al., 1983; Lotova et al., 1985) could be a signature of early destabilization of shear layers (Grappin et al., 1996), but also of acoustic (or more generally magnetoacoustic) waves dissipating there. (Note that Alfvén waves are not expected to show such a rapid dissipation). The aim of this paper is to study the interaction between acoustic waves and the wind in the region of the sonic point, in the simplest framework: the isothermal Navier-Stokes equations, with no radiation, no temperature stratification, no magnetic field.

Previous studies of the back-reaction of the acoustic waves on the mean flow were based on the equations for the Lagrangian-mean velocity (Jacques 1977; Pijpers and Hearn, 1989). These studies concluded that the flow is faster in presence of waves, We reconsider this problem, and find that the flow is actually in average slowed-down by outward propagating sound waves. The discrepancy is easily solved by taking into account the systematic drift (Stokes drift) between the absolute and the Lagrangian frame. We examine in the discussion which one of the two averaging procedures is appropriate when considering stellar winds or the solar wind. In any case, models based on the equations for the Lagrangian-mean velocities cannot, strictly speaking, be used to study large-amplitude waves and/or low-frequency waves: such limitations are absent when integrating directly the Navier-Stokes equations.

The velocity u and density ρ are assumed to be solutions of the Euler equations in the spherically symmetric, isothermal case:

$$\partial u/\partial t + u\,\partial u/dr + (c^2/\rho)\partial\rho/\partial r = -GM/r^2 \tag{1a}$$

$$\partial\rho/\partial t + \frac{1}{r^2}\partial/\partial r(r^2\rho\,u) = 0 \tag{1b}$$

where c is the (constant) sound velocity. A transonic wind close to the Parker solution is obtained by perturbing an isothermal atmosphere. The sonic point $r_s^\circ = GM/(2c^2)$ is located inside the numerical domain $[r^\circ, r_1]$ (otherwise, the velocity profile depends on the position of the numerical boundary (Grappin, Léorat, Lignères, work in progress)), and the waves incident at

the bottom are left free to escape from the domain. The radial profile of the wave energy (based on the rms velocity dispersion measured during a wave period at each point) and the mean wind speed are computed and compared to the quasilinear predictions.

The plan of the paper is as follows: Sect. 2 gives a quasi-linear analysis of the propagation of acoustic waves and momentum exchange with the mean flow. Section 3 presents the numerical method. Section 4 gives the numerical results and Sect. 5 the discussion.

2. Linear analysis

2.1. Wave evolution: WKB versus non-WKB analysis

Linearizing Eq. (1), one finds the equations for radially propagating acoustic waves (Parker, 1966):

$$\partial z^+/\partial t + V^+\partial z^+/\partial r = -u'/uV^-(z^+ + z^-)/2 \quad (2a)$$

$$\partial z^-/\partial t + V^-\partial z^-/\partial r = -u'/uV^+(z^+ + z^-)/2 \quad (2b)$$

where $z^\pm$ are the eigenmodes of the homogeneous case:

$$z^\pm = \delta u \pm c\delta\rho/\rho \quad (3)$$

In Eq. (2), $u' = \partial u/\partial r$ is the gradient of the unperturbed flow velocity and $V^\pm = u \pm c$ is the group velocity of the waves in the absolute frame.

The characteristic variables $z^\pm$ play here the role played by Elsässer variables for Alfvén waves (see Heinemann and Olbert, 1980; Velli et al., 1989). In the high-frequency limit, the mean velocity gradient u' may be neglected, and in that case only $z^\pm$ denote the amplitude of the two eigenmodes propagating respectively upward and downward. Consider now an upward propagating monochromatic wave; to first-order, all fields vary as $exp[ik(r - (u + c)t)]$, with a frequency in the solar frame $\omega^\circ = k(u+c)$. From Eq. (2b) we see that the z^- amplitude cannot remain zero; its relative amplitude is obtained by replacing as usual in Eq. (2b) $\partial/\partial t$ by $-i\omega^\circ$ and $\partial/\partial r$ by ik, which gives:

$$z^-/z^+ = -i\varepsilon/(1 + i\varepsilon) \approx -i\varepsilon$$

$$\varepsilon = 1/4u'/u(u + c)^2/(\omega^\circ c) \quad (4)$$

The expression for ε diverges when the frequency goes to zero; in this limit, the full expression $-i\varepsilon/(1 + i\varepsilon)$ should be used; it leads to $z^- = -z^+$, i.e. to $\delta u = 0$, $\delta\rho \neq 0$. Note also that the ε parameter decreases with distance to the sun: this is because $u'/u \approx 1/r^2$ at short distances, and $\approx 1/r$ at large distances.

The z^- amplitude given by Eq. (4) is that of the "anomalous" upward propagating wave while the "normal" z^- component (i.e., the one corresponding to the homogeneous case where $u' = 0$) is propagating downward (see Velli et al 1989). In conclusion, one should not necessarily interpret the amplitude of z^- as indicating a true reflection of the wave: when the ratio z^-/z^+ is equal to the expression given in Eq. (4), there is no reflection.

The anomalous upward propagating component z^- vanishes in the high-frequency (WKB) limit, as seen from Eq. (4). The usual WKB condition is that the wavelength of the wave be much shorter than the characteristic length of the medium, which would read here $u'/(ku) \ll 1$ or $u'/u(u + c)/\omega^\circ \ll 1$. We see from Eq. (4) that this is almost equivalent to the condition that $z^-/z^+ \ll 1$, apart from a factor $(u+c)/c$. In the WKB limit, one can derive from Eq. (2a) the invariance of the wave action (Parker, 1966; Jacques, 1977):

$$\mathrm{div}(\rho SV) = 0$$

The action is here defined as $S =< \delta u^2 > /\omega, \omega) = kc$ being the sound frequency in the plasma frame, and $V = u + c$ is the velocity of the outward propagating sound waves in the absolute frame. The action flux $\varepsilon = \rho SVr^2$ is thus constant. The frequency in the plasma frame ω is related to the frequency ω° in the absolute frame by $\omega = \omega^\circ c/(u+c)$. Using this relation and also the invariance of the mean mass flux $F^\circ = \rho ur^2$ to lowest order, the action flux reads:

$$\varepsilon = \rho r^2[< \delta u^2 > /(\omega^\circ c)](u + c)^2$$

$$\varepsilon = F^\circ/(\omega c) < \delta u^2 > (u + c)^2/u \quad (5a)$$

This may also be expressed as the following "WKB law" (Parker, 1966):

$$< \delta u^2 > \propto u/(u + c)^2 \quad (5b)$$

From this relation one infers that the radial wave energy profile follows two successive phases: in the quasi-static (strongly stratified) part of the atmosphere where $u \ll c$, the wave energy grows exponentially with distance:$< \delta u^2 > \propto u \propto 1/\rho$, while it decreases slowly at larger distances where $u > c$.

Equation (5) does not take into account either reflections or dissipation. When z^- becomes important, the conserved quantity is no longer the energy in the incident wave flux, but the net wave action flux (Velli, 1993):

$$\varepsilon^+ - \varepsilon^- = (1/(\omega^\circ c))\rho c^2 r^2[< \delta z^{+2} > (u + c)^2 - < \delta z^{-2} > (u - c)^2] \quad (6)$$

Equation (6) is not as useful as Eq. (5), since the value of z^- is unknown in general, except in the purely outward case where it is given by Eq. (4). When z^- is negligible but not dissipation, the action flux ε [see Eq. (5a)] is no longer constant; a possible generalization is then $\varepsilon = \varepsilon^\circ exp(-(r - r^\circ)/H)$, H being the characteristic dissipation length, and ε° being a constant (Jacques, 1977; also Pijpers and Hearn, 1989).

2.2. Back-reaction of the waves in the WKB approximation: slow-down of the mean flow

We compute now the variation of the mean wind speed due to a steady flux of acoustic waves incident at some point in the atmosphere. The hypotheses are the same as in Jacques's (1977) work: the amplitude of the wave is assumed small enough, so that the relative change in the mean flow velocity induced by

the waves is small, the nonlinear steepening of the waves is neglected. We start by taking the time-average (denoted by brackets) of Eq. (1) which gives the stationary equations:

$$< uu' > + c^2 < \rho'/\rho >= -GM/r^2 \tag{7a}$$

$$< \rho u r^2 >' = 0 \tag{7b}$$

where y' denotes the spatial derivative dy/dr. The velocity and density are the sum of their time-average (still denoted by u and ρ) and a fluctuating part δu and $\delta\rho$ with zero mean, so that the equations above become, to second order in the fluctuating quantities:

$$uu' + c^2\rho'/\rho + < \delta u\delta u' - c^2\delta\rho\delta\rho'/\rho^2 >= -GM/r^2 \tag{8a}$$

$$\rho'/\rho + u'/u + 2/r + d/dr[< \delta\rho\delta u > /(\rho u)] >= 0 \tag{8b}$$

Assume now that the fluctuations are outward propagating and take the high-frequency limit, i.e., assume $\delta u = c\delta\rho/\rho$. The fluctuating quantities disappear from the momentum Eq. (8a), while, in the continuity Eq. (8b), their contribution becomes $d/dr < \delta u^2/(uc) >$. The two equations are then combined to obtain an equation containing only u and δu:

$$u'/u(u^2 - c^2) - cd/dr(< \delta u^2 > /u) = 2c^2/r^2(r - r_s^\circ) \tag{9}$$

where $r_s^\circ = GM/(2c^2)$ is the sonic radius of the unperturbed wind. Equation (9) is to be compared with the equation for the Lagrangian-mean velocity v [see Eq. (3) in Pijpers and Hearn, 1989], also valid for high-frequency waves:

$$v'/v(v^2 - c^2) + v/2d/dr(< \delta u^2 > /v) = 2c^2/r^2(r - r_s^\circ) \tag{9'}$$

One sees that the waves contribute for terms with opposite signs in the Eqs. (9) and (9′). The origin of this difference is that there is a systematic drift v_d ("Stokes drift") between the ordinary and the Lagrangian frames, which depends on the amplitude of the waves (see Jacques, 1977):

$$u = v + v_d = v - < \delta u^2 > /c \tag{10}$$

This drift is large enough for the wave acceleration (as measured using Lagrangian means) to become a deceleration (using standard averages), an effect previously overlooked. It is not difficult to prove that Eqs. (9) and (9') are indeed equivalent, using Eq. (10) and the WKB relation [Eq. (5b)].

Note that the problem does not appear in the case of Alfvén waves, since in that case there is no drift between the Lagrangian and standard frames (Jacques, 1977). Also, in the Alfvén case, the direction of propagation is unimportant, the sign of the wave pressure is always the same. In the case of acoustic waves on the contrary, if we consider inward propagating waves, the sign of the correlation between density and velocity fluctuations changes, so that the wave "pressure" in Eq. (9) changes sign.

Let us examine the consequences of Eq. (9). In presence of waves, the sonic radius, i.e., the radius where $u = c$ in Eq. (9), becomes:

$$r_s \approx r_s^\circ - r_s^{\circ 2}/(2c)(< \delta u^2 > /u)'_{|r} = r_s^\circ \tag{11}$$

The sonic point is thus shifted outward wherever the wave energy is decreasing with distance.

To evaluate this shift, we must relate the wave energy profile to the unperturbed wind speed. From the approximate invariance of the action flux [Eq. (5a)], we obtain that $(< \delta u^2 > /u)' = -2\alpha^\circ cu'/(u + c)^3$, where $\alpha^\circ = \varepsilon^\circ\omega^\circ/F^\circ$, so that Eq. (11) becomes, using $u' \approx c/r_s^\circ$ to lowest order at the sonic point:

$$r_s - r_s^\circ \approx r_s^\circ\alpha^\circ/(8c^2) \approx r_s^\circ \frac{1}{2c^2} < \delta u^2 >_{|r=r_s^\circ} \tag{12}$$

showing that the increase of the sonic radius is directly proportional to the incident wave flux. To evaluate the relation between the mean velocity variation and the wave energy everywhere, we integrate Eq. (9), and obtain the following invariant, the mean "energy" E:

$$E = u^2/2 - c^2 1nu - c < \delta u^2 > /u - 2c^2 1nr - GM/r \ . \tag{13}$$

Let us denote by E_α and u_α the mean energy and velocity of the solution resulting from a given wave flux α, and by E° and u° the mean energy and velocity with zero flux. Evaluating the energies E_α and E° at a given radius r, we obtain from Eq. (13):

$$\begin{aligned} E_\alpha - E^\circ &= (u_\alpha^2 - u^{\circ 2})/2 - c^2 1n(u_\alpha/u^\circ) - c < \delta u^2 > /u_\alpha \\ &\approx u^\circ\Delta u - c^2\Delta u/u^\circ - c < \delta u^2 > /u^\circ \end{aligned} \tag{14}$$

where $\Delta u = u_\alpha - u^\circ$ is the mean velocity variation (at radius r) due to a wave flux α. Another expression for the energy difference, which does not contain Δu, may be found by evaluating E_α and E° respectively at the perturbed and unperturbed sonic radii, i.e., $E_\alpha(r = r_s)$ and $E^\circ(r = r_s^\circ)$. One obtains, by noting that the two terms $-2c^2 1n(r_s/r_s^\circ) - GM(1/r_s - 1/r_s^\circ)$ cancel to second order, independently of the detailed expression of the sonic radius (12):

$$E_\alpha - E^\circ \approx < \delta u^2(r = r_s^\circ) > \tag{15}$$

Combining Eqs. (14) and (15), and dropping the index $^\circ$ for the unperturbed velocity, we obtain:

$$\Delta u = \left(\frac{uc}{u^2 - c^2}\right)\left(\frac{< \delta u^2 >}{u} - \frac{< \delta u^2 >}{c}|_{r=rs^\circ}\right) \tag{16}$$

Using Eq. (5a) for the action flux to express the wave amplitude in terms of the unperturbed wind speed in Eq. (16), we obtain:

$$\Delta u = -\alpha^\circ \frac{u(u + 3c)}{4(u + c)^3} \tag{17a}$$

which shows that the velocity variation Δu grows with the base wave energy flux. An equivalent expression, showing the dependence on the local wave energy, is:

$$\Delta u = - < \delta u^2 > \frac{u + 3c}{4c(u + c)} \tag{17b}$$

We have in particular at the sonic point:

$$\Delta u = -\frac{\alpha^\circ}{8c} \tag{18a}$$

$$= -\frac{1}{2c} < \delta u^2 >_{|r=rs^\circ} \quad (18b)$$

and, far enough from the sonic point, taking the limit $u \gg c$ in Eq. (16):

$$\Delta u = -\frac{1}{4c} < \delta u^2 >= -\frac{1}{u} < \delta u^2 >_| \; r = rs^\circ \quad (19)$$

Note that by comparing Eqs. (17b) and (10) we can convince ourselves that the deceleration is indeed converted into an (apparent) acceleration when working in the Lagrangian frame. Indeed, the Stokes drift [Eq. (10)] between the Euler frame attached to the sun and the Lagrangian frame is always larger in absolute value than the deceleration [Eq. (17b)], as long as $u > -c/3$, which is always valid in the present limit of small amplitude waves.

Dissipation can increase the velocity change by increasing the gradient of the wave amplitude close to the critical point, as seen by examining Eq. (16) which is still valid in presence of wave dissipation. As mentioned above, the expression in Eq. (5) becomes then multiplied by a factor $\exp(-(r - r^\circ)/H)$, so that near the critical point, the velocity variation in Eq. (18a) due to the wave flux becomes

$$\Delta u = -\frac{\alpha^\circ}{8c}(1 + r_s^\circ/H)\exp(-(r_s^\circ - r^\circ)/H) \quad (20)$$

α° being the flux at the basis r°. The maximum amplitude of the velocity variation (fixing everything except H) obtains when the dissipation length H is equal to the distance between the critical point and the basis, $H = (r_s^\circ - r^\circ)r_s^\circ/r^\circ$; the velocity variation is then amplified by the factor $exp(-r^\circ/r_s^\circ)(1 + r^\circ/(r_s^\circ - r^\circ))$. This effect is thus substantial only when the dissipation is concentrated in a very short distance range near the critical point, which makes sense only when nonlinear steepening of the waves is important and concentrated in this distance range.

3. Numerics

3.1. Spatial differenciation, dissipation and temporal scheme.

We use compact finite differences, i.e., implicit schemes, to compute the spatial derivatives (see Lele, 1992). Their main interest is to substantially reduce the amplitude of the error, compared to explicit methods of the same order, while being faster than spectral methods. We chose fourth-order schemes on boundary points and six-order schemes on interior points.

Such a numerical scheme is not dissipative in itself, so that explicit dissipation has to be added in general to the Eq. (1a), in order to prevent spurious accumulation of energy at grid scale. Although strictly speaking the characteristics are difficult to define in presence of dissipative terms, in practice the method is still applicable to the viscous case, as shown in Poinsot and Lele (1992) (note however that the viscosity is set to zero at the boundaries). A kinematic viscosity ν is used, in front of a Laplacian dissipation term $(\Delta u)_r$, so that the momentum equation reads:

$$\partial u/\partial t + u\partial u/dr + (1/\rho)\partial P/\partial r + GM/r^2 = \nu(\partial^2 u/\partial r^2 + 2/r(\partial u/\partial r - u/r)) \quad (21)$$

The viscosity ν is fixed as follows. During the transition phase from a static atmosphere to a stationary wind, one imposes that the viscous time computed at grid scale, $\tau_{\rm dis} = (\nu k_{\rm max}^2)^{-1}$, is lower than the nonlinear time $\tau_{NL} = (k_{\rm max} u_{\rm max})^{-1}$, where $u_{\rm max}$ is the maximum velocity and $k_{\rm max} = (\pi/L)(N-1)$ is the maximum wavenumber, $L = r^1 - r^\circ$ being the size of the domain and N the number of grid points). Once a stationary wind is established, the viscosity can in practice be suppressed, the wind remaining stable. The same is true when a wave flux is added, as soon as the wave does not steepen during its propagation through the numerical domain. Only when significant steepening occurs during advection time, some viscocity has to be used, adapted now to the wave amplitude δu, so that the dissipation time $\tau_{\rm dis}$ is smaller than the nonlinear time based on the wave amplitude δu.

The temporal scheme is Adams-Bashforth second order with variable time-step, except for the first time step which for which we use second-order Euler. The time-step is a fraction $1/3$ (for $N = 128$) or $1/5$ (for $N = 512$) of the smallest of the dissipation time and of $(k_{\rm max}(u_{\rm max} + c))^{-1}$.

3.2. Boundary and initial conditions

In order to obtain a reasonable measure of the exchange of momentum between waves and the mean wind in a finite portion of space, we need to let the wave escape freely from the numerical domain. This means that the outgoing characteristics (which carry the information escaping from the domain) are computed from the primitive equations, while on the other hand, the ingoing characteristics which carry the information coming from the outside of the domain, have to be specified.

Let us recall briefly the method (Thompson, 1987). We first write the momentum and continuity Eq. (1) in matrix form:

$$\partial/\partial t \begin{pmatrix}\rho\\ u\end{pmatrix} + \begin{pmatrix}u & \rho\\ c^2/\rho & u\end{pmatrix}\partial/\partial r \begin{pmatrix}\rho\\ u\end{pmatrix} + \begin{pmatrix}2\rho u/r\\ GM/r^2\end{pmatrix} = 0$$

We then project the system on the left eigenvectors $X^\pm = (c, \pm\rho)$ of the matrix $M = \begin{pmatrix}u & \rho\\ c^2/\rho & u\end{pmatrix}$, so as to obtain two equations with well-defined direction of propagation (depending on the sign of the eigenvalues $\lambda_\pm = u \pm c$ of matrix M):

$$c\partial\rho/\partial t \pm \rho\partial u/\partial t + L^\pm + 2c\rho u/r \pm GM\rho/r^2 = 0 \quad (22)$$

where

$$L^\pm = (u \pm c)(c\partial\rho/\partial r \pm \rho\partial u/\partial r) \quad (23)$$

The characteristics $L^\pm$ will be said "outward" or "inward", depending on the sign of the associated eigenvalues $u \pm c$. The

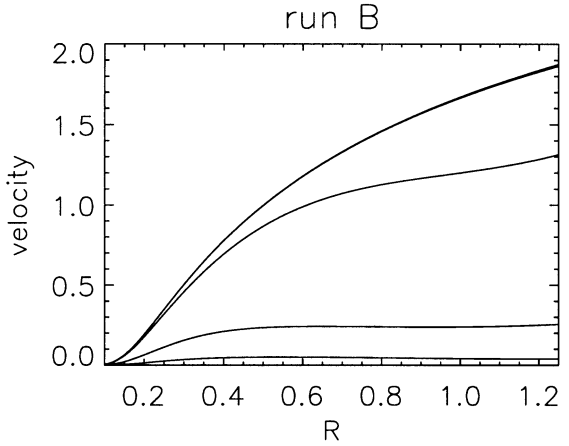

Fig. 1. Transonic wind formation by perturbation of a static atmosphere; successive radial profiles of the velocity at times $T = 0, 2, 4 \ldots 12$. (run B, $0.1 \leq r \leq 1.25$). The sonic point is at $r = 0.5$ (see text).

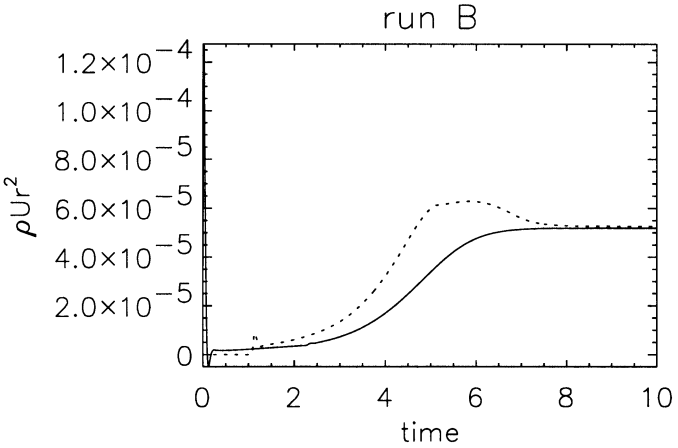

Fig. 2. Wind formation; mass flow $F = \rho u r^2$ through the bottom (continuous) and top (dotted) of the domain versus time (run B).

characteristic Eqs. (22-23) are exactly equivalent to the original Euler equations (1). Returning to the original variables, we obtain a third way of writing the Navier-Stokes equations:

$$\partial u/\partial t + (L^+ - L^-)/(2\rho) + GM/r^2 = 0 \tag{24a}$$

$$\partial \rho/\partial t + (L^+ + L^-)/(2c) + 2\rho u/r = 0 \tag{24b}$$

Equations (24) and (23) are equivalent to Eq. (1). The Eq. (1) are solved everywhere inside the domain $r^\circ < r < r_1$. At the boundaries, in all cases except when the flow is a supersonic outflow, the Navier-Stokes equations have to be modified to include the partial knowledge we have of the outside medium. This knowledge is propagated inside the numerical domain by the inward characteristics which will be replaced by convenient expressions (see below Eq. (27)), while the outward characteristics are computed according to their standard expressions in Eq. (23).

We start with an isothermal static atmosphere

$$u = 0, \rho = \rho^\circ \exp\{2r_s^\circ(1/r - 1/r^\circ)\} \tag{25}$$

where $r_s^\circ = GM/(2c^2)$ is the sonic radius. The numerical domain $[r^\circ, r^1]$ includes the sonic point. From Eq. (23) one derives the expressions of the characteristics at static equilibrium:

$$L^{-\circ} = -L^{+\circ} = \frac{\rho GM}{r^2} = -c^2 \frac{\partial \rho}{\partial r}_{|t=0} \tag{26}$$

This static equilibrium is perturbed at the inner boundary r° via the "inward" characteristics L^+ which is replaced by:

$$L^+ = -L^{-\circ}(r = r^\circ) + \delta L \quad (r = r^\circ) \tag{27a}$$

while at the outer boundary the inward characterisfics L^- is left unperturbed:

$$L^- = -L^{+\circ}(r = r_1) \quad (r = r_1) \tag{27b}$$

A negative δL leads to an acceleration of the fluid at the inner boundary. The perturbation propagates towards the outer boundary and leads to a breeze which grows with time (see next section). A new equilibrium forms, characterized by a transonic wind with $u = c$ at the expected radius $r = r_s^\circ$. At the inner boundary, the new stationary state is characterized by a density ρ^* and outward characteristic L^- which are solution of Eq. (24); in particular, the new equilibrium density is

$$\rho^* = \rho^\circ(1 + \Delta)/(1 + \frac{u^* r^\circ}{c r_s^\circ}) \quad (r = r^\circ) \tag{28}$$

where $\Delta = \delta L r^{\circ 2}/(2\rho^\circ c^2 r_s^\circ)$, $r_s^\circ = GM/(2c^2)$ is the sonic point and u^* is the transonic velocity at the inner boundary r°. It is seen that in the limit of vanishing perturbation $\delta L = 0$, and when the inner boundary is close to the surface ($r^\circ \ll r_s^\circ$), the final equilibrium density is identical to the static density.

Once the new equilibrium is reached, a constant flux of acoustic waves is added to the incoming characteristic at the inner shell:

$$L^+(t) = -L^{-\circ} + \delta L + A\omega^\circ \cos\omega^\circ(t - t^*) \quad (r = r^\circ, t \geq t^*) \tag{29}$$

and keeping the same condition (see Eq. (27b)) at the outer shell. The averages and standard deviations of various quantities are measured during one period $2\pi/\omega^\circ$. The amplitude of the incident wave depends not only on the parameters A and ω°, but also on the inner radius. Assume that the reflected component remains small, i.e., $\delta\rho/\rho = \delta u/c$. Using Eqs. (22) and (29) and linearizing, one obtains that the incident amplitude z^+ [see Eq. (3)] satisfies to

$$\partial \delta z^+/\partial t = -A\rho^\circ \cos\omega^\circ(t - t^*) - \beta \delta z^+ \tag{30}$$

where the coefficient $\beta = (u^\circ + c)/r^\circ + r_s^\circ c/r^{\circ 2}$ measures a damping associated with the curvature terms ($\beta \approx 13$ when $r^\circ = 0.1$). The solution of Eq. (30) reads:

$$\begin{aligned} \delta z^+(r^\circ, t) \quad &= A\rho^\circ\omega^\circ(\beta^2 + \omega^{\circ 2})^{-1}\{\beta \cos\omega^\circ(t - t^*) \\ &+\omega^\circ \sin(\omega^\circ(t - t^*) - \beta e^{-\beta(t-t^*}\} \end{aligned} \tag{31}$$

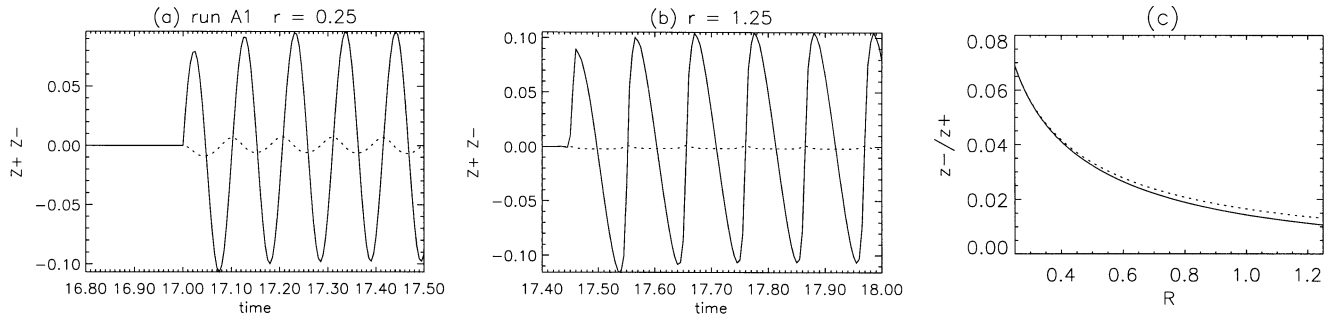

Fig. 3a–c. Incident and reflected wave amplitude $z^+ = \delta u \pm c\delta\rho/\rho$, versus time in a quasi-linear case (run A1). **a** bottom **b** top of the domain **c** profile versus distance of the ratio of rms amplitudes z^-/z^+ (continuous: simulation; dotted: Eq. (4)).

For a frequency of $\omega^\circ = 60$, Eq. (31) leads to a transient period of two oscillations before a stationary regime is reached. The rms amplitude of the wave at the inner shell reads after the transient phase:

$$\delta z^+_{\rm rms}(r^\circ) = (A\rho^\circ/\sqrt{2})[1 + (\beta/\omega^\circ)^2]^{-1}. \quad (32)$$

Unit density is ρ°, the initial density at the inner shell. The velocity unit is sound speed, the spatial unit is twice the sonic radius r_s° (i.e., $r_s^\circ = 0.5$). (In these units, the gravitational acceleration is $1/r^2$). Unit time is thus the time a sound wave takes to travel twice the sonic radius in the static atmosphere. A typical perturbation amplitude is $\delta L = -3$. We integrated up to $t = 13$ to obtain a stable wind, integrated further with zero viscosity up to $t = 17$, and input a steady flux of waves from $t = 17$ up to 20. A typical waveperiod is $T^\circ \approx 0.1$, corresponding to $\omega^\circ = 60$. Assuming $r_s^\circ = 10$ solar radii, and $c = 80$ km/s, the unit time is about $1.710^5 s$, hence $\omega^\circ = 60$ corresponds to a wave period in the absolute (or spacecraft's) frame about $T = 5$ hours.

We have considered several resolution and domain sizes. Table 1 gives a summary of the various runs and parameters.

4. Numerical results

4.1. Formation of the wind

We perturb the static isothermal atmosphere with a pressure and velocity perturbation [see Eq. (27a)] $\delta L = -3$. A breeze sets in, grows (see Fig. 1), and becomes a transonic wind. (Note that an explicit perturbation is actually not really necessary: the transonic wind also obtains by waiting a time long enough for the numerical errors to destabilize the initial static equilibrium). The fact that no stable breeze sets in due to the initial perturbation may be explained by pressure arguments: the inner pressure increase due to the perturbation δL cannot match the equilibrium conditions of any breeze solution, which all have pressure gradients lower than the static equilibrium (see Velli, 1994).

Figure 1 shows the velocity at times $t = 0, 2, \ldots 12$, showing the stabilization towards the transonic wind within the radial domain [0.1, 1.25] (run B). The asymptotic mass flux depends on δL [see Eq. (28)]; this is not surprising, as the density at either boundary is not fixed. The stationarity of the final state and also the precision of the calculations is shown by comparing (Fig. 2) the mass flux F at the inlet and outlet; it is defined as:

$$F = r^2\rho u. \quad (33)$$

The mass contained in the numerical domain first increases during a short period, and then decreases; it stabilizes finally around $T \approx 8$. At that time, the mass flux entering and leaving the domain should be about equal, the difference between the two fluxes being a measure of the precision of the computation. The largest flux variation is actually found between the inner boundary and the first interior grid point; the error is directly related to the relative jump in the static density profile between these two grid points. In the case of run B, shown in Fig. 2, the relative jump in the mass flux and in the density profile are respectively $\Delta F/F \approx 10^{-2}and\Delta\rho/\rho \approx 0.2$. In run C, the density slope at the bottom is smaller, so that $\Delta\rho/\rho \approx 0.08$ and $\Delta F/F \approx 10^{-4}$.

4.2. Small amplitude, high-frequency waves

We now inject a steady flux of acoustic waves at the bottom of the domain, once the transonic wind is established and stabilized. In order to compare with the quasi-linear expressions of Sect. 2, we first consider here a case where both steepening and non-WKB effects (measured by ε in Eq. (4)) are negligible. Steepening does not occur if the nonlinear time $1/(k\delta u)$ is larger than the transport time through the numerical domain, which is $\int dr/(u+c) \approx (1/\alpha)L/(u^\circ + c)$, where u° is the velocity at the bottom of the domain and $\alpha > 1$. Since the wave number k is related to the frequency ω° of the wave in the absolute frame by $\omega^\circ = \omega + ku = k(u + c)$, this condition becomes:

$$L\omega^\circ\delta u/(u^\circ + c)^2 < \alpha$$

We have seen that the wave amplitude δu is a function of A, ω° and r° (see Eq. (32)), so this relation is not very useful; in practice, one must check a posteriori that the condition is satisfied. In run A1 which we consider in this section, $L = 1$, the maximum wave amplitude is $\delta u = 0.04$, $\omega^\circ = 60$, and $u^\circ \approx 0.35$, so that $L\omega^\circ\delta u/(u^\circ + c)^2 \approx 1.3$. On the other hand, the ε parameter is 0.07 at the bottom and decreases with distance, as we have seen in Sect. 2.1.

Figure 3 shows the time evolution of the $z^\pm$ components at the bottom (Fig. 3a) and top (Fig. 3b) of the domain for run Al.

Table 1. List of runs, with parameters and main characteristics. Δr is the interval of radial distance defining the integration domain (the sonic point is $r_s^\circ = 0.5$). N is the number of grid points. ν is the viscosity. A is the amplitude of the forcing leading to the incident acoustic wave. ω° is the frequency. ζ is the maximum ratio $z^-_{\rm rms}/z^+_{\rm rms}$ (found at the bottom boundary). $\delta u^{\rm max}_{\rm rms}$ is the maximum rms amplitude of the acoustic wave. The velocity of sound is one.

Run	Δr	N	ν	A	ω°	ζ	$\delta u^{\rm max}_{\rm rms}$	Comments
A	0.25, 1.25	128	$2\ 10^{-3}$	0				
A1	———	—	10^{-5}	-0.1	60	0.07	0.04	WKB regime
B	0.1, 1.25	512	$2\ 10^{-3}$	0				
B1	———	—	10^{-5}	-1	10	1	0.09	Low frequency
B2	———	—	10^{-3}	-3	10	1	0.28	Shock above sonic point
B3	———	—	—	-0.2	60	0.32	0.22	Shock below sonic point
C	0.1, 0.9	1024	—	0				
C1	———	—	—	-0.4	60	0.32	0.34	Shock below sonic point

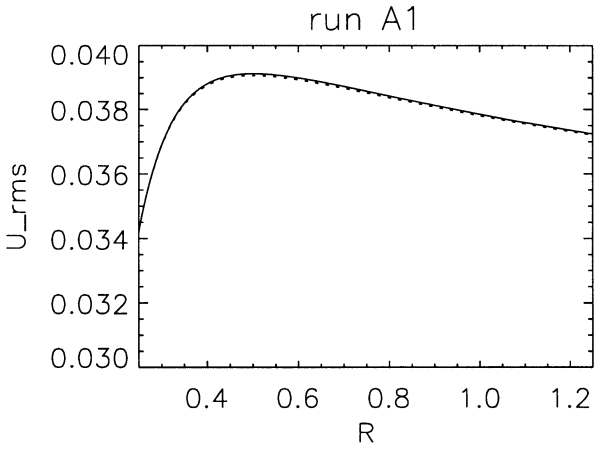

Fig. 4. Profile of rms wave amplitude $\delta u_{\rm rms}$ (run A1). (continuous) simulation result (dotted) Linear extrapolation of the wave profile from the inlet amplitude, using the WKB Eq. (5b).

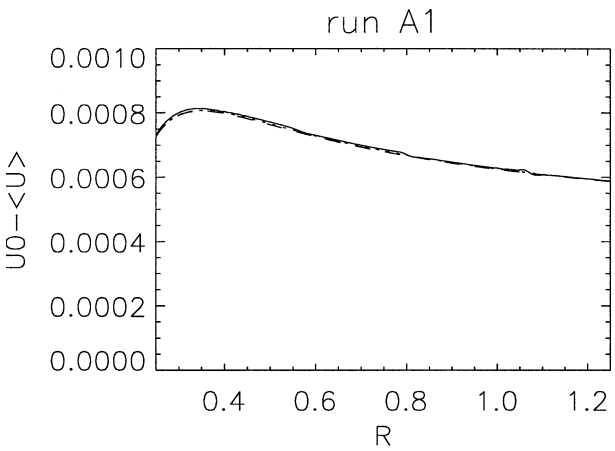

Fig. 5. Mean velocity variation due to the waves (run A1). (continuous) simulation result; (dotted) using Eq. (17b); (dashed) using Eq. (17a).

The amplitude of the minor component z^- is maximal at the inner boundary, and its oscillations follow those of the incident component z^+ with a $\pi/2$ phase delay, as predicted by Eq. (4). It is much smaller, and becomes spiky at the outlet; however, its amplitude is about exactly that predicted by Eq. (4); hence, reflection is negligible in this situation. The main component z^+ shows some steepening. The WKB invariant (Eq. (5)) is conserved within 2% (Fig. 4), and the mean velocity variation Δu predicted by Eq. (17) is very close to the numerical solution (Fig. 5).

4.3. Non-WKB waves; shocks

What happens when either the frequency is low, which might lead to reflections, or when the incident amplitude is large enough to lead to shocks? We consider in turn the two effects.

Consider run B1, $\omega^\circ = 10$, with the inner boundary at $r^\circ = 0.1$, $L = 1.15$. At such a low frequency, the parameter $\varepsilon \approx 2$ at the inner boundary (Eq. (4)). As shown by Fig. 6, the wavelength is indeed larger than the scale height. With an amplitude $A = -1$, the peak rms velocity amplitude is $\delta u \approx 0.09$, and the nonlinear steepening is not more apparent than in the previous run A1

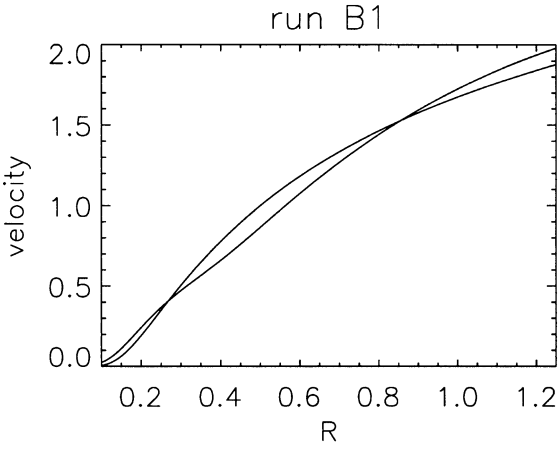

Fig. 6. Unperturbed and perturbed velocity profiles, run B1.

($L\omega^\circ\delta u/(u^\circ + c)^2 \approx 1$ in run B1). Figure 7 shows various average and rms profiles. Figure 7a shows the average and rms velocity. Figure 7b shows the mean mass flux $< F >=< \rho u > r^2$, (the dotted line shows the sole contribution of the average, $F^\circ =< \rho >< u > r^2$). Figure 7c shows the rms $z^\pm$ amplitudes; Fig. 7d the ratio z^-/z^+, which is seen to be about 1. This is

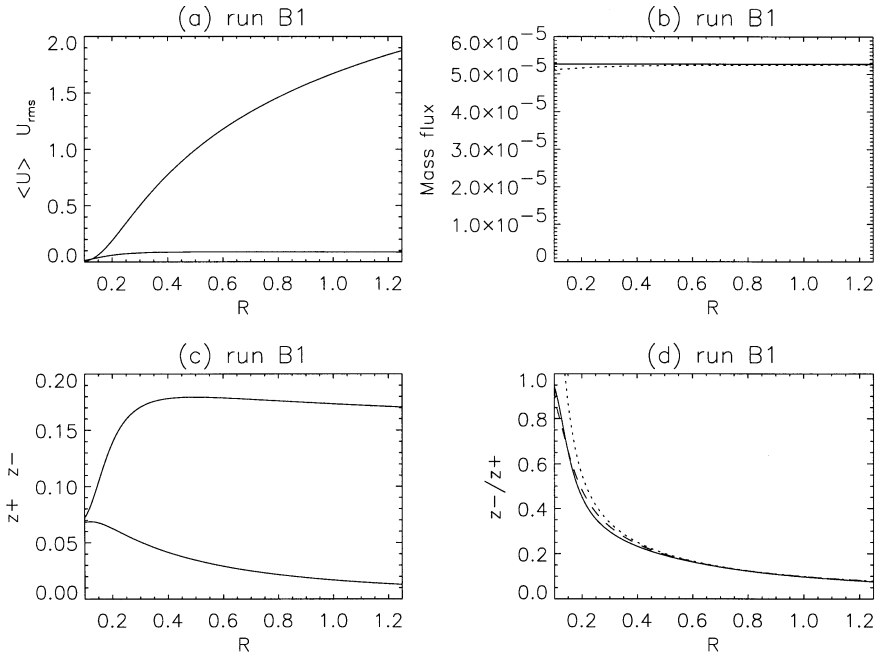

Fig. 7a–d. Averages and rms values, run B1. **a** Mean and rms velocity profile **b** Mean mass flux $< F >=< \rho u r^2 >$(continuous) and partial contribution $F^\circ =< \rho >< u > r^2$ (dotted) **c** rms amplitudes z^+ and z^- **d** ratio of rms amplitudes z^-/z^+ (continuous: simulation; dotted: linear approximation (Eq. (4)) $z^-/z^+ = -i\varepsilon$; dashed: full Eq. (4)).

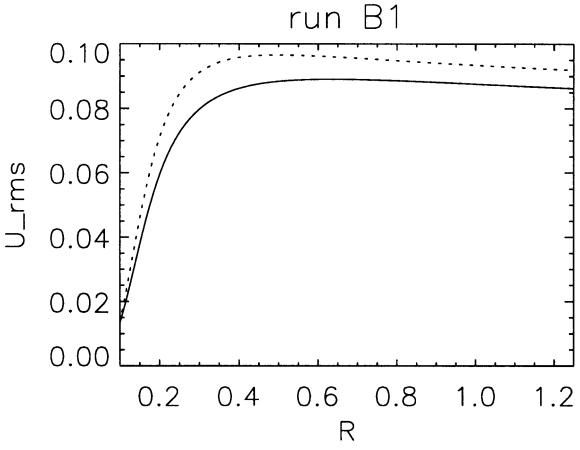

Fig. 8. Profile of rms wave amplitude $\delta u_{\rm rms}$ (run B1). Same legend as Fig. 4.

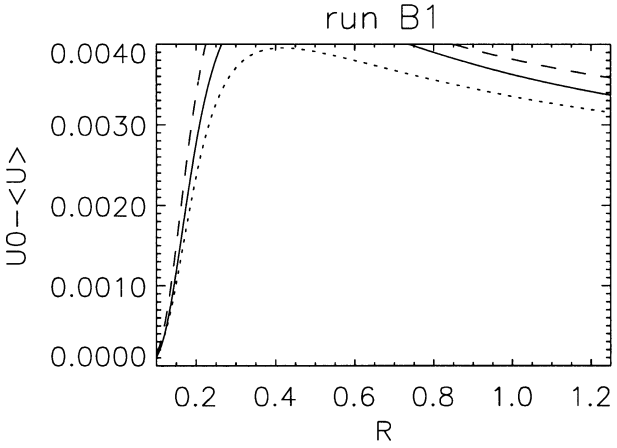

Fig. 9. Mean velocity variation due to the waves (run B1). Same legend as Fig. 5.

lower than ε, but about the value predicted by the full expression (Eq. (4)), showing again that reflection is negligible. Because the minor component z^- is important, the radial profile of the wave amplitude δu is substantially different from the WKB prediction (Fig. 8). But if one plots the full wave action (Eq. (6)), one obtains as expected a nearly constant curve, apart from a jump of about 0.5% observed on the first grid point. Finally, the measured mean velocity decrease due to the wave is very close to the one obtained via the hybrid formula (Eq. (17b)) which combines both the wave amplitude and the unperturbed wind speed, but deviates substantially from the one obtained via Eq. (17a) which depends only on the unperturbed wind speed, and overestimates the velocity decrease (Fig. 9).

More important changes are expected when one decreases the nonlinear time so that a shock forms within the domain. This is achieved by increasing either or both of the wave amplitude

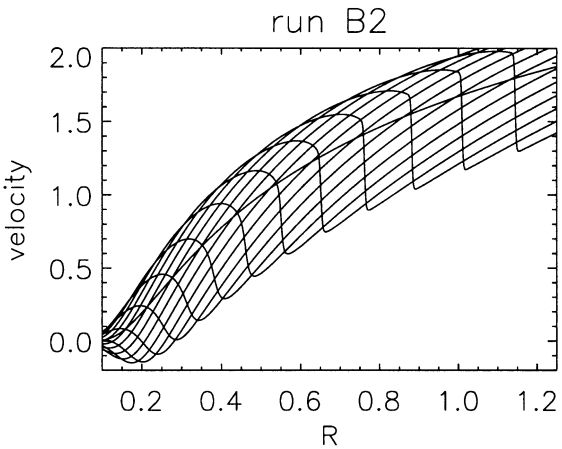

Fig. 10. Unperturbed and perturbed velocity profiles, run B2.

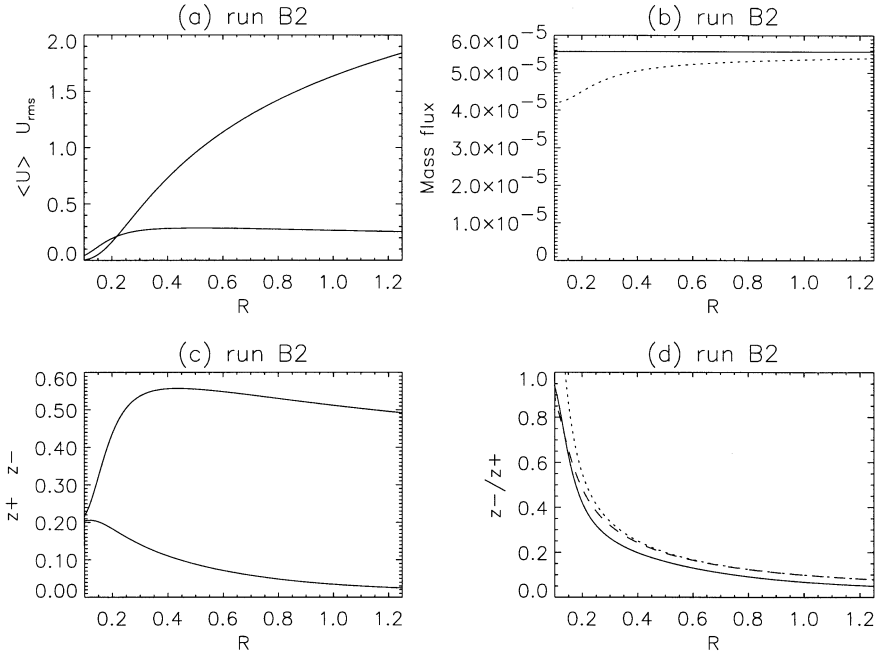

Fig. 11. Averages and rms values, run B2. Same legend as Fig. 7.

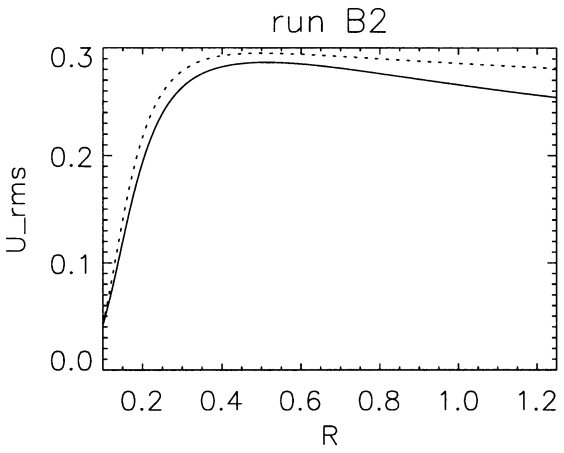

Fig. 12. Profile of rms wave amplitude $\delta u_{\rm rms}$ (run B2). Same legend as Fig. 4.

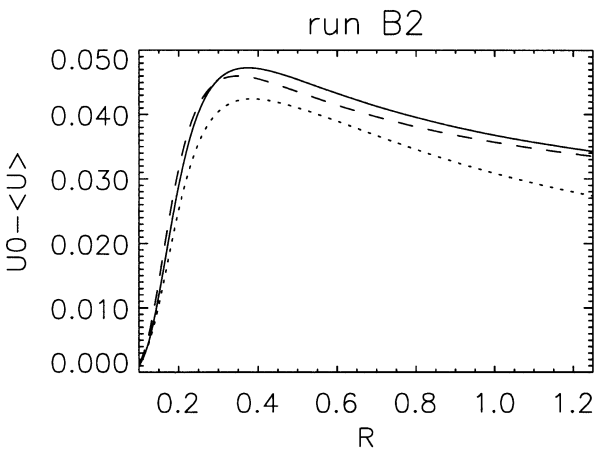

Fig. 13. Mean velocity variation due to the waves (run B2). Same legend as Fig. 5.

and the frequency. First consider the case of intermediate amplitudes and frequencies, where shock formation occurs in the supersonic region. Consider run B2 with an inlet rms velocity of $0.04 (A = -3)$; the frequency is $\omega^\circ = 10$ (Fig. 10). A viscosity of $\nu = 10^{-3}$ is necessary to correctly dissipate the shock. The rms velocity profile of the wave amplitude (Fig. 11 and 12) is flat, with a maximum $\delta u \approx 0.3$ near $r = 0.4$. The profile departs somewhat from the WKB prediction, due both to the low frequency (in the subsonic region), and to the dissipation of the shock in the supersonic region. For the same reason, there are some departure of the measured z^-/z^+ ratio from Eq. (4). This departure is maximum at the bottom boundary when using the linear formula ($z^-/z^+ = \varepsilon$, dotted line in Fig. 11d); but, again, using the full formula $|z^-/z^+| = \varepsilon/(1+\varepsilon^2)^{1/2}$ gives the correct value at the bottom (dashed line), as in the previous run (Fig. 7). However, the deviation persists at large distance, and increases in relative value. Hence, one cannot exclude that there is some reflection in this case. In spite of this, the mean velocity decrease follows qualitatively Eq. (17); the maximum velocity decrease reaches about 0.05 (Fig. 13).

If one decreases further the nonlinear time, a shock forms below the sonic point. Since the wave dissipates now in a low-speed region, the dissipation rate per unit distance is much increased compared to the preceding case. As a consequence, the wave profile becomes sharply peaked, which should lead to a stronger decrease of the mean velocity (see Eq. (16)). This is shown on two examples. Both have frequency $\omega^\circ = 60$. The first case (Fig. 14a) is run B3 ($u^\circ_{\rm rms} = 0.05, A = -0.2$); the second case (Fig. 14b) is run C1, with a wave amplitude twice as large. In both cases, there is a sharp maximum in the wave amplitude,

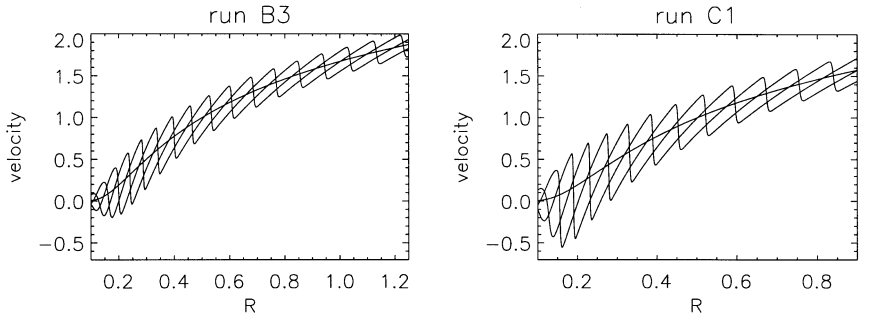

Fig. 14. Unperturbed and perturbed velocity profiles **a** run B3 **b** run C1.

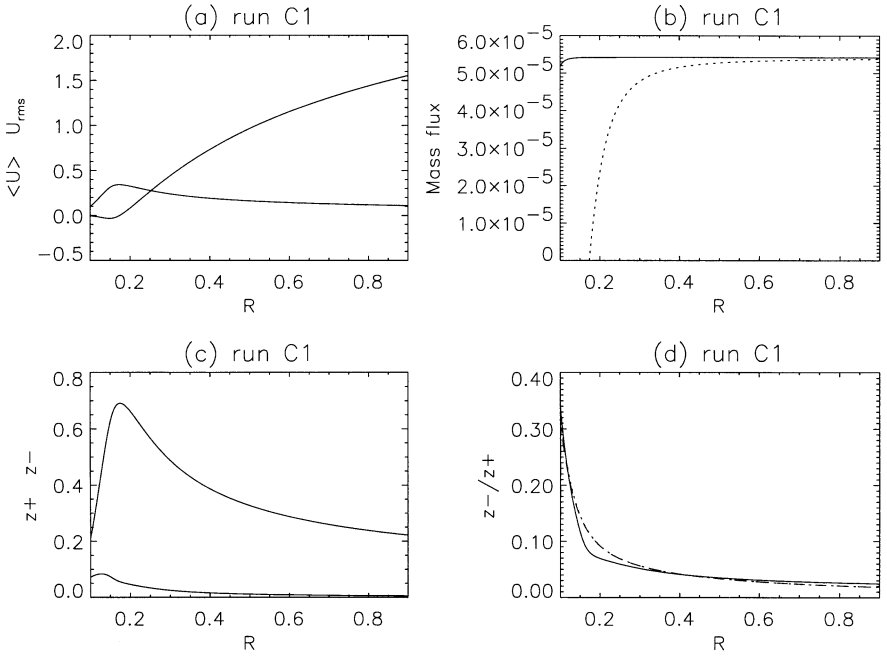

Fig. 15a–d. Averages and rms values, run C1. Same legend as Fig. 7.

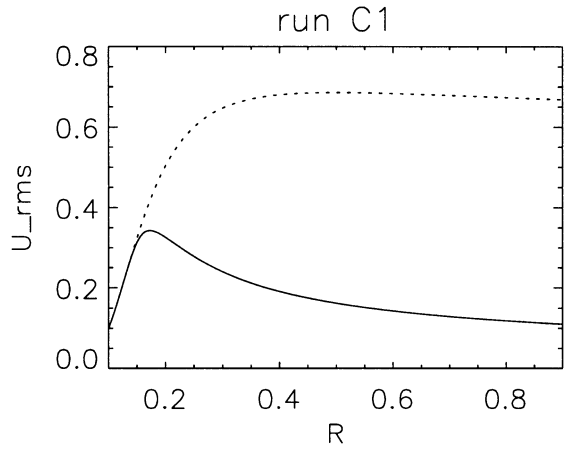

Fig. 16. Profile of rms wave amplitude $\delta u_{\rm rms}$ (run C1). Same legend as Fig. 4.

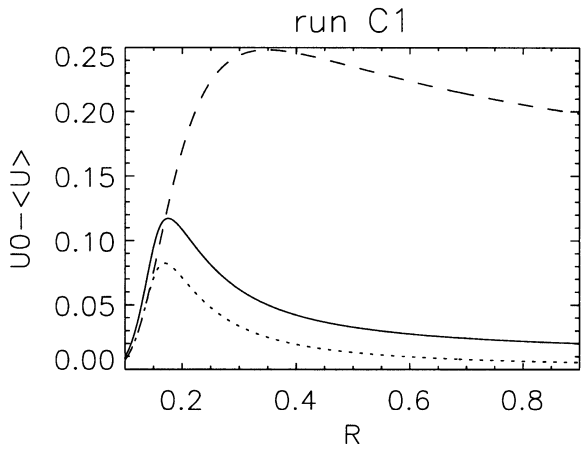

Fig. 17. Mean velocity variation due to the waves (run C1). Same legend as Fig. 5.

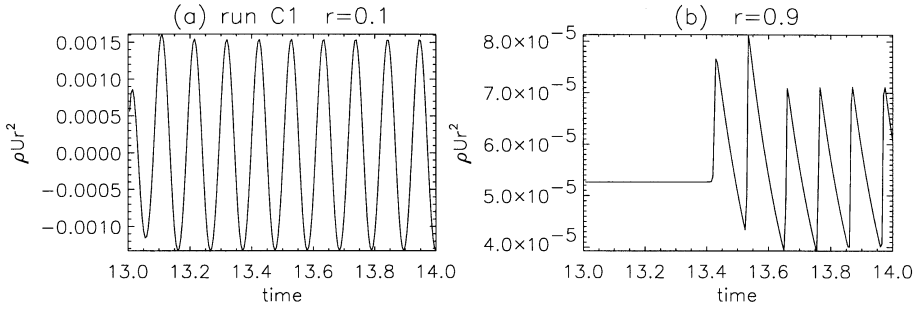

Fig. 18a and b. Mass flux at the bottom and top of the domain (run C1) versus time.

which was not visible in the previous runs. One also suspects by examining Fig. 14b that the mean velocity becomes negative in the subsonic region, in the case with largest wave amplitude. Figures 15 to 17 detail run C1. In Fig. 15, we see that the average velocity is indeed negative in the region [0.1, 0.2]. The ratio z^-/z^+ is surprisingly well fit by Eq. (4). On the other hand, the viscous dissipation leads to a strong departure from WKB prediction for the wave amplitude decrease (Fig. 16). Note that using the generalization by Jacques (1977) of the WKB invariant to take dissipation into account, $\delta u^2 \propto u/(u+c)^2 \exp(-(r-r^\circ)/H)$, does not help. Indeed, the dissipation length is much longer in the supersonic than in the subsonic region (due to the different advection speeds), so that it is impossible to fit the wave profile with a single dissipation length H; either the wave amplitude level is completely wrong, or the asymptotic decay law is wrong. Last, the mean velocity decrease is substantially larger than the quasilinear prediction, with a peak around $r \approx 0.15$, about the same location as the maximum in wave amplitude (Fig. 17). Note that the formula (Eq. (17b)), which is partially based on the real wave amplitude, still gives a reasonable fit, while Eq. (17a) is here largely overestimating the deceleration, because it does not take the wave dissipation into account.

It is important to remark that the transient phase lasts for several wave periods. During the first two wave periods, the momentum exchange between the mean flow and the wave leads to an *increase* in the average speed, in the two runs with large wave amplitudes, B2 and C1. This is illustrated in Fig. 18, which shows the mass flux variations at the bottom and top of the domain.

In the case with largest amplitude (run C1, $A = -0.4$, $\delta u_{\max} = 0.34$), the correct resolution of the wave profile has required to modify the numerical scheme, namely turning to a conservative form of the continuity equation, using a larger resolution $N = 1024$ instead of 512, spanning a smaller radial interval, [0.1, 0.9], and adding a small diffusion term $\eta = 2\,10^{-6}$ to the continuity equation. This artificial term was necessary to damp a long term instability associated with the conservative form of the continuity equation; it has the drawback to prevent exact balance of the mean mass flux close to the inner boundary, as seen in Fig. 15. It is important to note however that, the profiles of rms quantities are not basically different in the two runs B2 and C1.

5. Discussion

We have studied the propagation of acoustic waves incident on the bottom of an atmosphere through which blows a transonic wind in the isothermal case, motivated by the simplicity of the problem which allows an easy computation of both the propagation properties and the back-reaction on the flow.

We find that the effect of the mean velocity gradient on the waves is generally reduced to a small modification of the eigensolutions (Eq. (4)): in practice, there is no large reflection. We conjecture that this result might also hold for *radial* Alfvén waves propagating along a radial mean magnetic field. In the case of Alfvén waves, the normal eigenmodes of the homogeneous case are $z^\pm = u \pm b/\sqrt{\rho}$; they propagate in opposite directions along the mean magnetic field. If our conjecture is true, the main departure from a zero z^- component, as observed for instance in the simulations by Lau and Siregar (1996) would not be due to reflections, but to either a) the minimal anomalous component also propagating outward (see Velli et al., 1989) and/or b) the compressible component generated by the expansion (Grappin et al., 1993). This would imply that the substantial z^- component observed in the solar wind is generated by the largescale shear flows, absent from the mentioned simulations.

We find that after a transient acceleration phase, the flow speed reaches a value lower than that of the unperturbed flow, the deceleration being approximately proportional to the energy of the wave. In the limit of linear high-frequency waves, the simulation results correspond well to the analytical estimation (Eq. (17)). This deceleration is not contradictory with the standard assertion that waves always accelerate the wind (see Jacques, 1977), since the latter assertion concerns the Lagrangian velocity averages, not the temporal averages considered here. Which definition corresponds better to observations? In the limit of small amplitudes, the Lagrangian mean amounts to a density-weighted mean, and this can be somewhat generalized (Andrews and McIntyre, 1978), so that stellar wind velocities based on line profiles are close to Lagrangian-mean velocities (Pijpers, personal communication). In contrast, average velocities of solar wind streams measured by in situ probes and radio scintillations are ordinary averages, and furthermore the results of the integration of the primitive equations is clearly more straightforward in terms of standard averages, so that it is worth considering the problem in terms of the latter.

For high enough wave amplitudes, the relative deceleration is such that the average speed becomes negative below the sonic

point. This does not imply that the flow is accreting matter in average, since the average mass flux is positive and independent of the radial distance. Let us give a short intuitive demonstration of why, in presence of large-amplitude waves propagating upward in an atmosphere, the mean flow velocity has to be negative somewhere. The main point is the positive correlation which exists between density and velocity fluctuations in an acoustic wave which is propagating upward. Particles oscillate back and forth with respect to the local frame of reference (which is advected at the average wind velocity). If the amplitude is large, there are many more particles (per unit volume) which oscillate upward than the reverse. If nothing else happened, this would lead to an enhanced upward flux of particles. But the (average) mass flux is independent of distance. In particular, its value at large distances is close to its unperturbed value, since there the wave amplitude is small. In other words, the average mass flux cannot be much enhanced by the presence of waves. Hence the only way out, for the average mass flux in the region of large wave amplitude to remain unchanged, is to have an average velocity much lower than the unperturbed one, and possibly negative.

The preceding argument works more generally for compressive waves propagating close to the radial direction. One may conjecture that in the MHD framework, large quasi-radial acoustic-like waves also lead to lower or negative average velocities, while Alfvén waves lead to larger-than-average velocities. This could lead to a criterion for determining the nature of the fluctuations in the region of solar wind acceleration or below, where no direct in situ measurements have been done up to now.

Since there is no drift between the Lagrangian frame and the normal frame in the case of Alfvén waves (Jacques, 1977), the concept of wind acceleration by the gradient of Alfvén waves flux (Alazraki and Couturier, 1971; Belcher, 1971; Hollweg, 1973; Lau and Siregar, 1996) remains independent of the definition we take for the mean velocity. The different back-reaction of acoustic and Alfvén waves on the average flow might play a role in the latitudinal gradients in the velocity observed in the heliosphere: low latitudes exhibit slower velocities than the higher latitudes. Low latitudes show, close to the sun, closed magnetic structures, while higher latitudes show more often open structures. It is not unphysical to imagine that the closed structures more easily generate sound-like waves (due to the bending of field lines, which couples Alfvén and compressive waves), while the open regions are a source of Alfvén waves. Hence, following the conclusion of this work, one expects the average speed close to the equatorial region to be decreased compared to its "unperturbed" value, while at higher latitudes the flow would be accelerated by Alfvén waves to larger values. The investigation of the consistent nonlinear-coupling between the wind, compressive and transverse fluctuations is an important objective of further work in the same direction.

Acknowledgements. We warmly thank J. Léorat and A. Mangeney for many fruitful discussions, and F. Pijpers for pertinent criticism of the manuscript.

References

Alazraki, G., Couturier, P.: 1971, Astron. and Astrophys. **13**, 380
Andrews, D.G., McIntyre, M.E.: 1978, J. Fluid Mech. **89**, 609
Belcher, J.W.: 1971, Astrophys. J. **168**, 509
Belcher, J.W., Davis, L.Jr.: 1971, J. Geophys. Res. **76**, 3534
Grappin, R., Léorat, J., Cavillier, E., Prigent, G.: 1997, Astron. Astrophys. **317**, L31
Hollweg, J.V.: 1973, Astrophys. J. **181**, 547
Jacques, S.A.: 1977, Astrophys. J. **215**, 942
Korevaar, P., Van Leer, B.: 1988, Astron. Astrophys. **200**, 153
Lau, Y.T., Siregar, E.: 1996 **465**, 451–461
Lele, S.K.: 1992, J. Comput. Phys. **103**, 16–42
Lotova, N.A., Blums, D.F., Vladimirsky, K.N.: 1985, Astron. Astrophys. **150**, 266
Parker, E.N.: 1958, Astrophys. J. **128**, 664
Parker, E.N., Dynamical theory of the solar wind, Space Sci. Rev. **4**, 666, 1965
Parker, E.N.: 1966, Astrophys. J. **143**, 32
Pijpers, F.P., Hearn, A.G.: 1989, Astron. and Astrophys. **209**, 198–210
Poinsot, T.J., Lele, S.K.: 1992, J. Comput. Phys. **101**, 104–129
Scott, S.L., Coles, W.A., Bourgois, G.: 1983, Astron. and Astrophys. **123**, 207
Thompson, K.W.: 1987, J. Comput. Phys. **68**, 1–15
Velli, M., Grappin, R., Mangeney, A.: 1989, Phys. Rev. Lett. **63**, 1807
Velli, M., Grappin, R., Mangeney, A.: 1991, Geophys. Astrophys. Fluid Dyn. **54**, 101–122
Velli, M.: 1993, Astron. Astrophys. **270**, 304
Velli, M.: 1994, Astrophys. J. **432**, L55

This article was processed by the author using Springer-Verlag LaTeX A&A style file *L-AA* version 3.